Preprints of the 21st IFAC World Congress (Virtual)
Berlin, Germany, July 12-17, 2020

Development of a HiL Load Simulator for Experimental Investigation of Translational Oscillating Systems

Abd Elkarim Masoud *, **Robert Courant** *, **Jürgen Maas** *

* *Mechatronic Systems Laboratory, Technical University of Berlin, Berlin, Germany, e-mail: abdelkarim.masoud@emk.tu-berlin.de*

Abstract: In this paper, the principle of a hardware in the loop (HiL) load simulator is applied on an amplitude-controlled translational oscillatory actuator (TOA). For this purpose, an electromechanical actuator is designed and build, that can emulate different oscillating load characteristics. To describe the system, consisting of a translational oscillatory actuator and the HiL actuator, a nonlinear model is derived. Next, a general averaged model is set up comprising several time-varying Fourier coefficient. The controller is based on a linearized averaged model and considers a multi variable structure to control both amplitude and phase of the applied force. Finally, the concept is validated using simulations and experiments. The results show, that the designed controller with the realised hardware can robustly emulate a desired load on an amplitude-controlled TOA under investigation. Because of its high sensitivity to temperature, a force measurement using strain gauges was not applicable. Instead, the output equation of the nonlinear state space model was used to estimate the load force.

Keywords: nonlinear averaged model, force and amplitude control, nonlinear oscillatory systems, multivariable control, decoupling control, describing function theory, translational oscillatory actuator (TOA).

1. INTRODUCTION

Translational electromechanical transducers are used in a wide range of application because of their high power density, simple structure, low mechanical loss and good controllability. These actuators generate translational movements directly without mechanical deflection and are increasingly used in industry and are present in various domains, such as automotive industry, electrical machines, robotic applications and household devices, see Haiwei et al. (2008) and Leonhard (2003). A special form of translational electric drives are translational oscillatory actuators. They are used for example in engines to reduce the caused vibration and noise Choi et al. (2017), in active vibration control of drum type washing machine Suzuki et al. (2017), vibration suppression in the process of plating, coating or rolling of steel sheets to avoid problems of deformation, peeling and non-uniform products and many other applications, see Sudwilai et al. (2011) . Another important application of translational oscillatory actuators is the medical and cosmetic skin treatment which use an oscillating needle to punctuate the human skin repetitively without risking complications in deeper tissue layers, see Sperry (1991).

For such applications a controlled electrodynamic vibration actuator was designed, see Mönnich (2018), which enables an energy-efficient resonance operation via mechanical springs. Furthermore, an amplitude and vibration controlled translational drive was investigated in Masoud (2019), where instead of mechanical springs magnetic springs have been used to reduce the mechanical losses.

In order to test these and other novel translational actuators and their control under load conditions, a suitable test setup is required. A test of controllers can be done according to Borgeest (2014) via the hardware-in-the-loop method. This method is typically used in automotive systems and will be applied to the amplitude-controlled translational oscillatory actuator (TOA) presented in Masoud (2019). In this paper a hardware-in-the-loop (HiL) translational actuator is developed, which applies a defined load on the tested amplitude-controlled TOA. Thus, a force-controlled translational actuator is designed, which can reproducibly exert adjustable load characteristics on an amplitude-controlled actuator. A force control is required in order to compensate the external disturbances and the deviating parameters of the HiL actuator. The use of a versatile test bench not only allows fast modification of different load configurations, since it offers also the possibility of automated long term tests.

For a model-based control design, a nonlinear dynamic model for the HiL-actuator is presented taking into account the amplitude-controlled translational actuator. Since we are working with oscillating systems, the nonlinear dynamic system is transformed into an averaged model using the approach presented in Sanders (1991). Thus, the fast changing quantities of the system are represented by their slowly time-varying Fourier coefficients. Furthermore, the nonlinear elements in the model are approximated using the describing function theory. Based on this model, a multivariable controller is designed taking into account the different objectives to control the coupling force between the HiL-actuator and the tested

translational actuator. Feedback information is generated by a position sensor of the slider, a force sensor to measure the coupling force and two current sensors. Besides the design of the developed HiL-actuator, especially modelling aspects and the design of the control will be presented in detail. Measurements gained by a real time system will be used to validate the proposed approach for the force controlled HiL-actuator.

The paper is structured as follows. The design and mathematical model (nonlinear state space model) for the HiL-actuator system is derived in chapter 2. The state-space averaged model of the nonlinear system is presented in chapter 3 and a multivariable controller is designed in chapter 4 to control the coupling force between the HiL-Actuator and the amplitude-controlled TOA. The experimental results shown in chapter 5 validate the proposed method, and chapter 6 summarizes the findings.

2. HARDWARE IN THE LOOP TRANSLATIONAL ACTUATOR (HIL-ACTUATOR)

2.1 Design of the HiL-Actuator

The design of the HiL-actuator system is shown in Fig. 1. The active component is a voice-coil-actuators (VCA) which generates the actuation force F_H. The VCA is rigidly coupled to an adjustable magnetic spring. It consists of axially magnetized permanent magnets and concentrically wounded coils inside the stator. Thus, the stiffness characteristic of the magnetic spring can be electrically changed. The springs provide a restoring force when the sliders

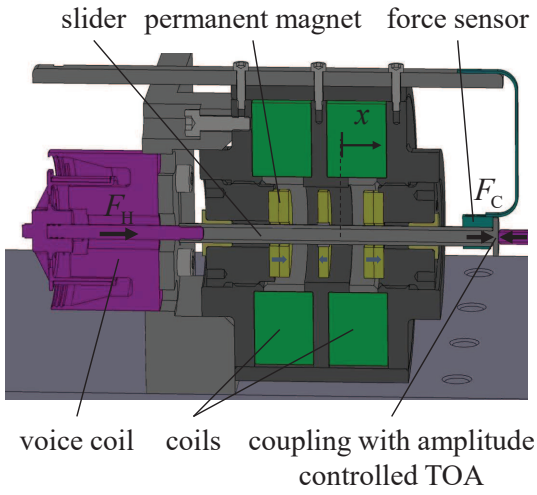

Fig. 1. Design of the HiL-actuator with magnetic spring elements.

are displaced, such that operation in resonance becomes possible. This is required in the considered application to keep the electrical power loss as small as possible and thus to limit the heating of the device. The increased efficiency is especially relevant for long-term investigation. A force sensor is installed between the HiL actuator and the amplitude-controlled TOA to measure the coupling force F_C and a laser triangulation sensor is used to detect the position x of the slider.

2.2 Mechanical model

The electromechanical system is modelled as a one mass oscillator consisting of the HiL-actuator and the amplitude-controlled TOA. Both actuators are suspended by magnetic springs, whose stiffnesses are approximated as third-order polynomials $F_{\mathrm{s,H}}(x), F_{\mathrm{s,A}}(x)$ with the general expression

$$F_\mathrm{s} = F_{\mathrm{s}0} + F_{\mathrm{s}1}x + F_{\mathrm{s}2}x^2 + F_{\mathrm{s}3}x^3 \tag{1}$$

and are also subject to Columb friction $F_{\mathrm{f,H}}(\dot{x}), F_{\mathrm{f,A}}(\dot{x})$

$$F_\mathrm{f} = \bar{F}_\mathrm{f}\,\mathrm{sgn}(\dot{x}). \tag{2}$$

Fig. 2 shows the mechanical model consisting of the HiL-actuator and the amplitude-controlled TOA.

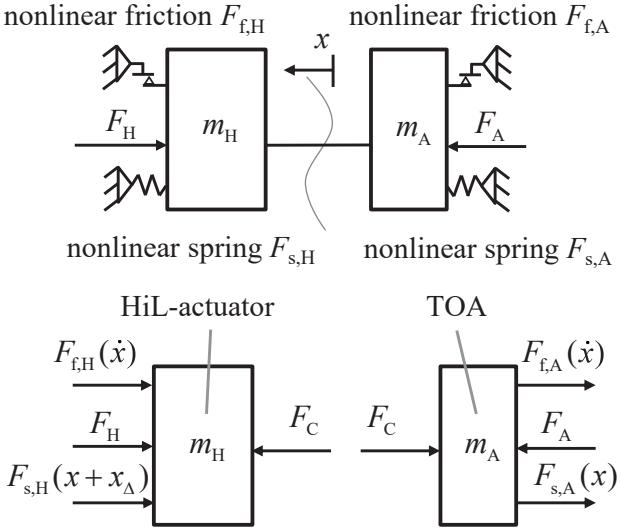

Fig. 2. Mechanical model of the HiL-actuator combined with the amplitude-controlled TOA.

The current supplied to the amplitude-controlled TOA generates the force F_A and is used to control the amplitude of the oscillation, see Masoud (2019). The mechanical model of the overall system which includes the two masses can be described by the nonlinear differential equation:

$$\begin{aligned}(m_\mathrm{H}+m_\mathrm{A})\,\ddot{x} = &-F_{\mathrm{s,H}}(x+x_\Delta) - F_{\mathrm{f,H}}(\dot{x}) - F_{\mathrm{s,A}}(x)\\ &- F_{\mathrm{f,A}}(\dot{x}) - F_\mathrm{H} + F_\mathrm{A}.\end{aligned} \tag{3}$$

The Hil actuator is shifted by x_Δ to obtain a constant coupling force F_C without external actuation while the offset position of the amplitude-controlled TOA remains at zero and is therefore considered in the equation by $F_{\mathrm{s,H}}(x+x_\Delta)$.

The coupling force F_C is obtained by separating the system into tow parts, as shown in the below part of Fig. 2. The consideration can in principle be made using the left or right single mass system. Since the HiL-actuator is considered in this paper and will be used for different amplitude-controlled TOA, it is useful to set up the differential equation of the left subsystem

$$\begin{aligned}&m_\mathrm{H}\ddot{x} = F_\mathrm{C} - F_{\mathrm{s,H}}(x+x_\Delta) - F_{\mathrm{f,H}}(\dot{x}) - F_\mathrm{H}\\ \Leftrightarrow\ &F_\mathrm{C} = m_\mathrm{H}\ddot{x} + F_{\mathrm{s,H}}(x+x_\Delta) + F_{\mathrm{f,H}}(\dot{x}) + F_\mathrm{H}.\end{aligned} \tag{4}$$

Equation (4) describes how the coupling force can be calculated without using a sensor to measure it. In this case we just need to measure the position x of the slider,

which is used for the amplitude-controlled TOA, and the force F_H generated by the VCA. Based on (3) and (4) a nonlinear state space model can be derived. For this purpose, the state vector, input, output and disturbance signals $\mathbf{x}, u, y, z$ are defined as

$$\begin{aligned} \mathbf{x} &= [\, x \;\; \dot{x} \,]^T = [\, x_1 \;\; x_2 \,]^T \\ u &= F_\mathrm{H}, \quad y = F_\mathrm{C}, \quad z = F_\mathrm{A} \end{aligned} \tag{5}$$

describing the nonlinear state space model by:

$$\begin{aligned} \dot{\mathbf{x}} &= \mathbf{f}\left(\mathbf{x}, u, z\right) \\ y &= g\left(\mathbf{x}, u, z\right), \end{aligned} \tag{6}$$

with

$$\begin{aligned} \mathbf{f}\left(\mathbf{x}, u, z\right) &= \begin{bmatrix} x_2 \\ -F_{\mathrm{s,H}}(x_1 + x_\Delta) - F_{\mathrm{f,H}}(x_2) \ldots \\ \ldots - F_{\mathrm{s,A}}(x_1) - F_{\mathrm{f,A}}(x_2) - u + z \end{bmatrix}, \\ g\left(\mathbf{x}, u, z\right) &= m_\mathrm{H}\dot{x}_2 + F_{\mathrm{s,H}}(x_1 + x_\Delta) + F_{\mathrm{f,H}}(x_2) + u. \end{aligned} \tag{7}$$

In order to express the output equation only with state variables $\mathbf{x}, u, z$ the state $\dot{x}_2$ in $g\left(\mathbf{x}, u, z\right)$ is expressed with the second equation in $\mathbf{f}\left(\mathbf{x}, u, z\right)$.

3. STATE-SPACE AVERAGED MODEL OF THE NONLINEAR SYSTEM

In the following chapter, a dynamically averaged model of the nonlinear system in (7) is developed in which the fundamental quantities of the HiL-actuator can be described in terms of their dynamic behaviour. It is assumed, that all state variables present in the system are sinusoidal with constant frequency whose amplitude and phase change only slowly in comparison within the oscillation period. The approach described in Sanders (1991) is applied, by which a state-space model is transformed into a generalized averaged model, so that instead of highly dynamic state variables only the slowly varying Fourier coefficients of the fundamental oscillation appear in the model.

First of all, the nonlinear system of differential equations is transferred to the state-space form (see chapter 2)

$$\begin{aligned} \dot{\mathbf{x}} &= \mathbf{f}\left(\mathbf{x}, u, z\right) \\ y &= g\left(\mathbf{x}, u, z\right). \end{aligned} \tag{8}$$

With the assumption of periodical state variables, the quantities of $\mathbf{x}$, u and z can be represented by their Fourier series with time-varying Fourier coefficients

$$\begin{aligned} x_i(t) &= x_i^0(t) + \sum_{k=1}^{\infty} x_{ik}^\mathrm{c}(t)\cos\left(k\omega_\mathrm{e}t\right) + x_{ik}^\mathrm{s}(t)\sin\left(k\omega_\mathrm{e}t\right), \\ u(t) &= u^0(t) + \sum_{k=1}^{\infty} u_k^\mathrm{c}(t)\cos\left(k\omega_\mathrm{e}t\right) + u_k^\mathrm{s}(t)\sin\left(k\omega_\mathrm{e}t\right), \\ z(t) &= z^0(t) + \sum_{k=1}^{\infty} z_k^\mathrm{c}(t)\cos\left(k\omega_\mathrm{e}t\right) + z_k^\mathrm{s}(t)\sin\left(k\omega_\mathrm{e}t\right). \end{aligned} \tag{9}$$

The amplitudes of the higher harmonics are damped by the low-pass behaviour of the resonant system. Thus, only a few Fourier coefficients are required to approximate the state variables. Due to the resonance mode of the translational drive, it is sufficient to include only the DC-component and the first fundamental oscillation for the averaged model

$$\begin{aligned} x_1(t) &= x_1^0(t) + x_1^\mathrm{c}(t)\cos\left(\omega_\mathrm{e}t\right) + x_1^\mathrm{s}(t)\sin\left(\omega_\mathrm{e}t\right), \\ x_2(t) &= x_2^0(t) + x_2^\mathrm{c}(t)\cos\left(\omega_\mathrm{e}t\right) + x_2^\mathrm{s}(t)\sin\left(\omega_\mathrm{e}t\right), \\ u(t) &= u^0(t) + u^\mathrm{c}(t)\cos\left(\omega_\mathrm{e}t\right) + u^\mathrm{s}(t)\sin\left(\omega_\mathrm{e}t\right), \\ z(t) &= z^\mathrm{c}(t)\cos\left(\omega_\mathrm{e}t\right) + z^\mathrm{s}(t)\sin\left(\omega_\mathrm{e}t\right). \end{aligned} \tag{10}$$

The force of the amplitude-controlled TOA $z(t) = F_\mathrm{A}(t)$ has no DC-components $z^0(t) = F_\mathrm{A}^0(t)$, since the DC-component of the position $x(t)$ is already determined or controlled by the DC-component of the force $u^0(t) = F_\mathrm{H}^0(t)$ of the VCA.

The coefficients $x_1^0(t)$, $x_1^\mathrm{c}(t)$, $x_1^\mathrm{s}(t)$, $x_2^0(t)$, $x_2^\mathrm{c}(t)$, $x_2^\mathrm{s}(t)$, $u^0(t)$, $u^\mathrm{c}(t)$, $u^\mathrm{s}(t)$, $z^\mathrm{c}(t)$ and $z^\mathrm{s}(t)$ of the harmonic approximation are slowly varying quantities of time compared to the fast changing variables of the original state, input and disturbance quantities $\mathbf{x}(t)$, $u(t)$ and $z(t)$. The time derivatives of the state variables in (10) are given in case of a constant excitation frequency ω_e by

$$\begin{aligned} \frac{\mathrm{d}}{\mathrm{d}t}x_1(t) &= \frac{\mathrm{d}}{\mathrm{d}t}x_1^0(t) + \left(\frac{\mathrm{d}}{\mathrm{d}t}x_1^\mathrm{c}(t) + \omega_\mathrm{e}x_1^\mathrm{s}(t)\right)\cos\left(\omega_\mathrm{e}t\right) \\ &\quad + \left(\frac{\mathrm{d}}{\mathrm{d}t}x_1^\mathrm{s}(t) - \omega_\mathrm{e}x_1^\mathrm{c}(t)\right)\sin\left(\omega_\mathrm{e}t\right), \\ \frac{\mathrm{d}}{\mathrm{d}t}x_2(t) &= \frac{\mathrm{d}}{\mathrm{d}t}x_2^0(t) + \left(\frac{\mathrm{d}}{\mathrm{d}t}x_2^\mathrm{c}(t) + \omega_\mathrm{e}x_2^\mathrm{s}(t)\right)\cos\left(\omega_\mathrm{e}t\right) \\ &\quad + \left(\frac{\mathrm{d}}{\mathrm{d}t}x_2^\mathrm{s}(t) - \omega_\mathrm{e}x_2^\mathrm{c}(t)\right)\sin\left(\omega_\mathrm{e}t\right). \end{aligned} \tag{11}$$

The new state, input and disturbance vectors $\mathbf{x}_\mathrm{a}$, $\mathbf{u}_\mathrm{a}$, $\mathbf{z}_\mathrm{a}$ of the system are obtained using the Fourier coefficients for harmonic approximation with

$$\begin{aligned} \mathbf{x}_\mathrm{a} &= \left[\, x_1^0 \;\; x_1^\mathrm{c} \;\; x_1^\mathrm{s} \;\; x_2^0 \;\; x_2^\mathrm{c} \;\; x_2^\mathrm{s} \,\right]^T \\ \mathbf{u}_\mathrm{a} &= \left[\, u^0 \;\; u^\mathrm{c} \;\; u^\mathrm{s} \,\right]^T \\ \mathbf{z}_\mathrm{a} &= \left[\, z^\mathrm{c} \;\; z^\mathrm{s} \,\right]^T. \end{aligned} \tag{12}$$

For the right side of the state space model (6), the vector function $\mathbf{f}$ and the output function g must also be approximated by the first harmonics. For this purpose, the nonlinear elements of the state space model (friction and spring) are approximated using the describing function theory presented in Gelb (1968) and finally substituting the fundamental oscillation of the state space model. The describing function of the spring nonlinearity is determined by substituting the first equation of (10) in (1). Using the trigonometric identities, the products of the trigonometric functions can be described by there harmonics. Since only the first fundamental is considered here, the higher harmonics are neglected and it results in

$$F_\mathrm{s}\left(x_1^0, x_1^\mathrm{c}, x_1^\mathrm{s}\right) \approx F_\mathrm{s}^0 + F_\mathrm{s}^\mathrm{c}\cos(\omega_\mathrm{e}t) + F_\mathrm{s}^\mathrm{s}\sin(\omega_\mathrm{e}t) \tag{13}$$

with

$$\begin{aligned} F_\mathrm{s}^0 &= F_{\mathrm{s}0} + F_{\mathrm{s}1}x_1^0 + F_{\mathrm{s}2}\left(x_1^0\right)^2 + F_{\mathrm{s}3}\left(x_1^0\right)^3 \\ &\quad + \frac{1}{2}\left(F_{\mathrm{s}2} + 3F_{\mathrm{s}3}x_1^0\right)X_1^2 \\ F_\mathrm{s}^\mathrm{c} &= F_{\mathrm{s}1} + 2F_{\mathrm{s}2}x_1^0 + 3F_{\mathrm{s}3}\left(x_1^0\right)^2 + \frac{3}{4}F_{\mathrm{s}3}X_1^2x_1^\mathrm{s} \\ F_\mathrm{s}^\mathrm{s} &= F_{\mathrm{s}1} + 2F_{\mathrm{s}2}x_1^0 + 3F_{\mathrm{s}3}\left(x_1^0\right)^2 + \frac{3}{4}F_{\mathrm{s}3}X_1^2x_1^\mathrm{c}, \end{aligned} \tag{14}$$

where $X_1 = \sqrt{x_1^{\mathrm{c}^2} + x_1^{\mathrm{s}^2}}$ is the amplitude of the fundamental oscillation of the position $x_1 = x$. Since the spring

nonlinearity in the HiL-actuator $F_{\mathrm{s,H}}$ has an additional DC-component x_Δ the DC-component $\hat{x}_1$ in (14) is replaced by $x_1^0 + x_\Delta$ to compute the describing function of $F_{\mathrm{s,H}}$.

Next, the describing function of the Columb friction is determined by substituting the second equation of (10) in (2) according to Gelb (1968). The constant velocity x_2^0 occurs only during a short settling time and is otherwise zero, since we would get a permanent drift in the position, which is blocked by the magnetic springs of the actuator system. Thus, we get the fundamental oscillation of the friction without $\hat{x}_2$ as

$$F_{\mathrm{f}}\left(x_2^{\mathrm{c}}, x_2^{\mathrm{s}}\right) = F_{\mathrm{f}}^{\mathrm{c}} \cos(\omega_{\mathrm{e}} t) + F_{\mathrm{f}}^{\mathrm{s}} \sin(\omega_{\mathrm{e}} t) \tag{15}$$

with

$$\begin{aligned} F_{\mathrm{f}}^{\mathrm{c}} &= \frac{4\bar{F}_{\mathrm{f}}}{\pi} \frac{x_2^{\mathrm{c}}}{X_2} \\ F_{\mathrm{f}}^{\mathrm{s}} &= \frac{4\bar{F}_{\mathrm{f}}}{\pi} \frac{x_2^{\mathrm{s}}}{X_2} \end{aligned} \tag{16}$$

where $X_2 = \sqrt{x_2^{\mathrm{c}2} + x_2^{\mathrm{s}2}}$ is the amplitude of the fundamental oscillation of the velocity $x_2 = \dot{x}$.

The right hand side of (6) can now be approximated by substituting (10), (13) and (15) in $\mathbf{f}$, g and collecting DC-component, sin- and cos-terms

$$\begin{aligned} f_1\left(\mathbf{x}_{\mathrm{a}}, \mathbf{u}_{\mathrm{a}}, \mathbf{z}_{\mathrm{a}}\right) &= x_2^0 + x_2^{\mathrm{c}} \cos(\omega_{\mathrm{e}} t) + x_2^{\mathrm{s}} \sin(\omega_{\mathrm{e}} t) \\ f_2\left(\mathbf{x}_{\mathrm{a}}, \mathbf{u}_{\mathrm{a}}, \mathbf{z}_{\mathrm{a}}\right) &= f_2^0 + f_2^{\mathrm{c}} \cos(\omega_{\mathrm{e}} t) + f_2^{\mathrm{s}} \sin(\omega_{\mathrm{e}} t) \\ g\left(\mathbf{x}_{\mathrm{a}}, \mathbf{u}_{\mathrm{a}}, \mathbf{z}_{\mathrm{a}}\right) &= g^0 + g^{\mathrm{c}} \cos(\omega_{\mathrm{e}} t) + g^{\mathrm{s}} \sin(\omega_{\mathrm{e}} t) \end{aligned} \tag{17}$$

where f_2^0, f_2^{c}, f_2^{s}, g^0, g^{c} and g^{s}, are long nonlinear functions depending on $\mathbf{x}_{\mathrm{a}}, \mathbf{u}_{\mathrm{a}}, \mathbf{z}_{\mathrm{a}}$.

Finally, the left and right side in (6) are approximated by (11) and (17). In this case the DC-components, cos- and sin-terms on the left and right side are compared with each other so that we obtain the extended nonlinear averaged model

$$\begin{aligned} \frac{\mathrm{d}}{\mathrm{d}t}\mathbf{x}_{\mathrm{a}} &= \begin{bmatrix} x_2^0 \\ x_2^{\mathrm{c}} - \omega_{\mathrm{e}} x_1^{\mathrm{s}} \\ x_2^{\mathrm{s}} + \omega_{\mathrm{e}} x_1^{\mathrm{c}} \\ f_2^0\left(\mathbf{x}_{\mathrm{a}}, \mathbf{u}_{\mathrm{a}}, \mathbf{z}_{\mathrm{a}}\right) \\ f_2^{\mathrm{c}}\left(\mathbf{x}_{\mathrm{a}}, \mathbf{u}_{\mathrm{a}}, \mathbf{z}_{\mathrm{a}}\right) - \omega_{\mathrm{e}} x_2^{\mathrm{s}} \\ f_2^{\mathrm{s}}\left(\mathbf{x}_{\mathrm{a}}, \mathbf{u}_{\mathrm{a}}, \mathbf{z}_{\mathrm{a}}\right) + \omega_{\mathrm{e}} x_2^{\mathrm{c}} \end{bmatrix}, \\ \mathbf{y}_{\mathrm{a}} &= \begin{bmatrix} F_{\mathrm{C}}^0 \\ F_{\mathrm{C}}^{\mathrm{c}} \\ F_{\mathrm{C}}^{\mathrm{s}} \end{bmatrix} = \begin{bmatrix} g^0\left(\mathbf{x}_{\mathrm{a}}, \mathbf{u}_{\mathrm{a}}, \mathbf{z}_{\mathrm{a}}\right) \\ g^{\mathrm{c}}\left(\mathbf{x}_{\mathrm{a}}, \mathbf{u}_{\mathrm{a}}, \mathbf{z}_{\mathrm{a}}\right) \\ g^{\mathrm{s}}\left(\mathbf{x}_{\mathrm{a}}, \mathbf{u}_{\mathrm{a}}, \mathbf{z}_{\mathrm{a}}\right) \end{bmatrix} \end{aligned} \tag{18}$$

The Fourier-coefficients in (18) are time-varying in case of an excitation (modulation). The condition in which the fast-variables sine- and cosine terms can be shortened and thus the model can be balanced demands that the modulation frequency ω_{m} (change of the Fourier coefficients) must be smaller than the half excitation frequency $\omega_{\mathrm{e}}/2$, see Sanders (1991). The simulation with the averaged model (18) developed here provides the envelopes of the translational drive vibration signals. The output equation $\mathbf{y}_{\mathrm{a}}$ in (18) can be alternatively used to estimate the coupling force F_C similarly to (4).

4. CONTROL DESIGN OF THE HIL-ACTUATOR

Using the averaged model (18) a multi-variable decoupling PI-controller is designed, see Maas (2000). Fig. 3 shows the control structure considering a MIMO decoupling structure. The slowly varying Fourier coefficients of the VCA force $\mathbf{u}_{\mathrm{a}}$ must first be converted to the actual Force F_{H} by modulation, and the Fourier coefficients of the fundamental oscillation for the position x_1^0, x_1^{c}, x_1^{s} and the coupling force F_{C}^0, $F_{\mathrm{C}}^{\mathrm{c}}$, $F_{\mathrm{C}}^{\mathrm{s}}$ are obtained from the measured variables by phase-sensitive demodulation. The DC-, cos- and sin-components of the coupling force can be set independently of each other, thus creating a multivariable control system for each controlled variable. The multivariable system is internally coupled. This means

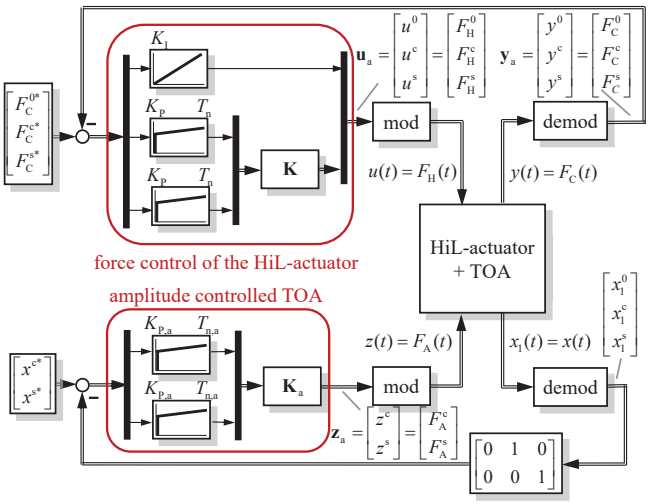

Fig. 3. Force and amplitude MIMO-control structure.

that each input can have an effect on each output. To avoid this and still be able to use SISO controller for a multivariable system, a decoupling controller is implemented. By this, the cross-couplings are suppressed and simple SISO-control loops can be designed for the controlled variable $F_{\mathrm{C}} = F_{\mathrm{C}}^0 + F_{\mathrm{C}}^{\mathrm{c}} \cos(\omega_{\mathrm{e}} t) + F_{\mathrm{C}}^{\mathrm{s}} \sin(\omega_{\mathrm{e}} t)$ as similar proposed in Maas (2000). In this paper we will not discuss the amplitude control, see Masoud (2019). For the force controller design, the nonlinear averaged model described in chapter 3 is first linearised at an equilibrium state $\mathbf{x}_{\mathrm{a,e}}$, $\mathbf{u}_{\mathrm{a,e}}$, $\mathbf{z}_{\mathrm{a,e}}$

$$\begin{aligned} \Delta\dot{\mathbf{x}}_{\mathrm{a}} &= \mathbf{A}\Delta\mathbf{x}_{\mathrm{a}} + \mathbf{B}\Delta\mathbf{u}_{\mathrm{a}} + \mathbf{B}_{\mathrm{z}}\Delta\mathbf{z}_{\mathrm{a}} \\ \Delta\mathbf{y}_{\mathrm{a}} &= \mathbf{C}\Delta\mathbf{x}_{\mathrm{a}} + \mathbf{D}\Delta\mathbf{u}_{\mathrm{a}} + \mathbf{D}_{\mathrm{z}}\Delta\mathbf{z}_{\mathrm{a}} \end{aligned} \tag{19}$$

with

$$\begin{aligned} \Delta\mathbf{x}_{\mathrm{a}} &= \mathbf{x}_{\mathrm{a}} - \mathbf{x}_{\mathrm{a,e}}, \\ \Delta\mathbf{u}_{\mathrm{a}} &= \mathbf{u}_{\mathrm{a}} - \mathbf{u}_{\mathrm{a,e}}, \\ \Delta\mathbf{z}_{\mathrm{a}} &= \mathbf{z}_{\mathrm{a}} - \mathbf{z}_{\mathrm{a,e}}, \end{aligned} \tag{20}$$

$$\begin{aligned} \mathbf{A} &= \frac{\partial \mathbf{f}_{\mathrm{a}}}{\partial \mathbf{x}_{\mathrm{a}}}, \quad \mathbf{B} = \frac{\partial \mathbf{f}_{\mathrm{a}}}{\partial \mathbf{u}_{\mathrm{a}}}, \quad \mathbf{B}_{\mathrm{z}} = \frac{\partial \mathbf{f}_{\mathrm{a}}}{\partial \mathbf{z}_{\mathrm{a}}}, \\ \mathbf{C} &= \frac{\partial \mathbf{g}_{\mathrm{a}}}{\partial \mathbf{x}_{\mathrm{a}}}, \quad \mathbf{D} = \frac{\partial \mathbf{g}_{\mathrm{a}}}{\partial \mathbf{u}_{\mathrm{a}}}, \quad \mathbf{D}_{\mathrm{z}} = \frac{\partial \mathbf{g}_{\mathrm{a}}}{\partial \mathbf{z}_{\mathrm{a}}}. \end{aligned}$$

For a simplified control design, linear springs are assumed.

With this simplification and neglecting the disturbance, we get the transfer function

$$\mathbf{G}_\mathrm{a} = \mathbf{C}_\mathrm{a}\left(s\mathbf{I} - \mathbf{A}_\mathrm{a}\right)^{-1}\mathbf{B}_\mathrm{a} + \mathbf{D}_\mathrm{a}$$
$$\mathbf{Y}_\mathrm{a} = \begin{bmatrix} G_{11} & 0 & 0 \\ 0 & G_{22} & G_{23} \\ 0 & -G_{23} & G_{22} \end{bmatrix} \mathbf{U}_\mathrm{a}. \tag{21}$$

The transfer function matrix (21) has symmetry properties, which further simplifies the controller design. Due to the simplified structure of the matrix, the DC component is already decoupled and therefore an I-controller is sufficient for the subsystem G_{11}. Furthermore the lower 2×2-matrix is antisymmetric and can be transformed into a block diagonal structure of the form

$$\mathbf{G}_\mathrm{d} = \begin{bmatrix} G_{22} & 0 \\ 0 & G_{22} \end{bmatrix}. \tag{22}$$

To achieve this, the 2×2 transfer function matrix is multiplied by the stationary decoupling matrix

$$\mathbf{K} = \begin{bmatrix} K_{22} & -K_{32} \\ K_{32} & K_{22} \end{bmatrix}. \tag{23}$$

The stationary decoupling is more than sufficient, as the resulting transfer function of the decoupled system is an identity matrix for frequencies up to a cut-off frequency, which is higher than the modulation frequency of the Fourier coefficients. The elements of the matrix (22) are identical, which is useful for the controller synthesis, since the same controller can be used for both parts of the system, so that a PI-controller can be designed by pole-placement for G_{22}. Through this multivariable decoupling controller, we are able to set the components of the coupling force F_C^{0*}, F_C^{c*}, F_C^{s*} (see Fig. 3).

5. EXPERIMENTAL RESULTS

To test the developed concept, the prototype depicted in Fig. 4 has been realized. The adjustable magnet spring as described in section 2.1 is dimensioned to compensate the effect of the HiL-actuator and emulate a light spring load. The remaining force difference can be set using the commercial voice coil actuator. The movement is induced by the amplitude control of the TOA under investigation. To measure the coupling force, a lightweight and stiff sensor had to be added. This has been achieved with semiconductor strain gauges bonded directly to the axis. First tests of the sensor showed a high sensitivity to temperature, which superimposed the strain dependency. Because of that, the coupling force in the following results is estimated according to (4). The averaged model of the translational drive system and the multivariable decoupling control structures were first designed using Matlab/Simulink and, in a second step, transferred to the real-time system MicroLabBox from dSPACE using compiled code. Parametrization of the controller and initialization of the set-point values as well as the recording of measurement signals are performed using the dSPACE tool ControlDesk.

To validate the designed HiL-actuator, certain tests have been conducted. One of those is depicted in Fig. 5. On the left, envelope curves of the oscillations are displayed and on the right, short time periods as marked with rectangles are shown. The upper plot illustrates the position of the rotor and the middle plot depicts the coupling force. Both visualize the measured signals and the respective set point

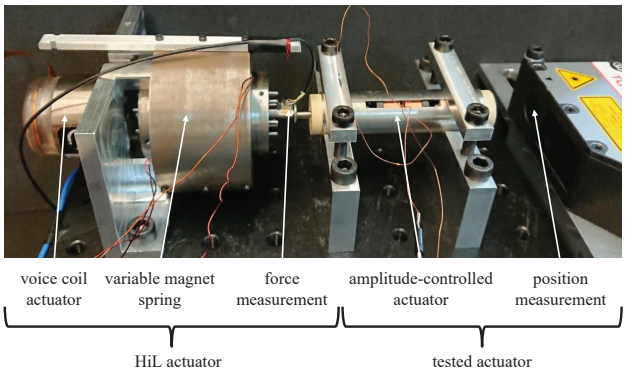

Fig. 4. Physical implementation of the system consisting of the HiL-actuator mechanically coupled with an amplitude-controlled TOA.

values. In the lower plot the actuation forces of both actuators are shown.

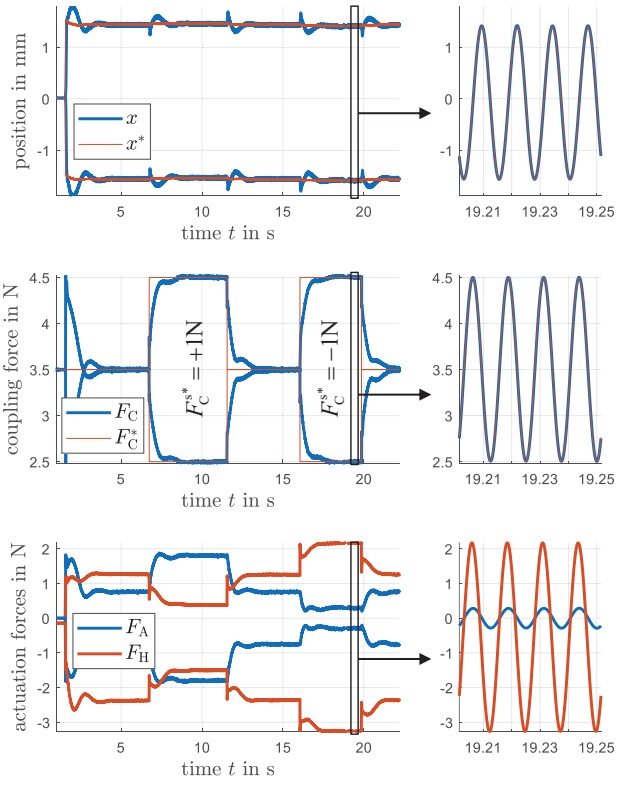

Fig. 5. Measured envelope curves and short period of oscillation of position, coupling force and actuation forces for different set point values.

The force control of the HiL-actuator is activated all the time. The constant component of the set point is always set to 3.5 N. The harmonic components vary in the experiment as described below. The amplitude control of the tested actuator is set to a cosine with 1.5 mm after 1 second and remains at this value in the following.

After 7 seconds, a sine-component of 1 N is added to the set point for the coupling force. This results in an increased actuation force for the cosine movement of the amplitude-controlled TOA. After 12 seconds, the oscillatory component of the coupling force is removed again and only the constant component remains. The sine-component of −1 N

after 17 seconds reduces the necessary actuation force of the tested actuator. The time signal of the actuation force shows, that both actuators operate in phase while they worked against each other between 7 and 12 seconds. The top plots show, that both control variables always reach there set points in amplitude and phase after a short settling time. This behaviour proves the load emulation capability of the HiL-system with the estimated coupling force. The position in Fig. 5 shows an overshooting for each change in the set points of the coupling force. This is caused by an interaction of the amplitude control of the TOA and the force control of the HiL-actuator, that occurs as uncompensated disturbances due to each other.

Having shown the emulation using the estimated coupling force, the compensation of the HiL-actuators influence on the coupling force can also be analysed in a more direct way by comparing the decoupled amplitude-controlled TOA with the same actuator coupled to the compensated HiL-actuator. The HiL-actuator is compensated when the set point of the coupling force has no varying components, as a constant part is necessary to prevent a lift-off of the coupling. In Fig. 6, the actuation force of the amplitude-controlled TOA set to 1 mm amplitude is shown coupled to the compensated HiL-actuator and without the HiL-actuator. After a short transition phase, both cases are expected to be identical for a full compensation. After 0.4 s, the decoupled actuator is switched on and the compensation is added to the already moving coupled system, resulting in a reaction in both amplitude curves.

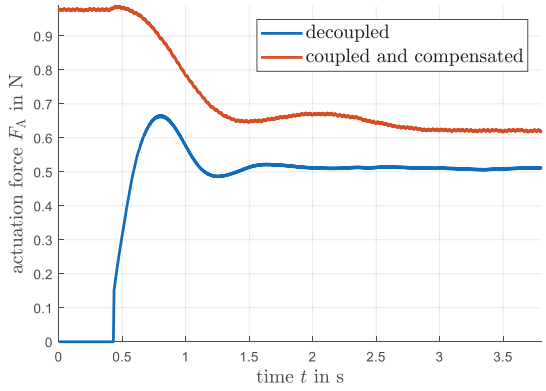

Fig. 6. Envelope curve of the actuation force of the amplitude-controlled TOA without HiL-actuator and coupled to the HiL-actuator set to a constant coupling force of 3.5 N.

It is obvious, that the compensation reduces the necessary actuation forces of the amplitude-controlled actuator. This is an expected result, as the dissipation of the HiL-actuator is now compensated by itself instead of the tested actuator.The remaining difference in the stationary result is caused by the estimation of the coupling force according to (4) that depends on the exact knowledge of the system behaviour. Especially, the friction can change significantly depending on the positioning.

6. CONCLUSION

In this paper an force decoupling controller was proposed to control the coupling force between the HiL-actuator and the amplitude-controlled TOA. For this purpose, a mechanical model of the translational drive system was presented. Thus, a nonlinear generalized averaged state space model was derived for the system, by which the highly dynamic state variables of the physical model can be replaced with there slowly time varying Fourier coefficients of the fundamental oscillation. Based on this model, the design and evaluation of multivariable decoupling PI-controllers was presented using the linearised averaged model and transforming it into the Laplace domain. Taking into account this model and symmetry properties of the transfer functions, the complexity of the controller design could be significantly reduced and thus a standard PI controller could be applied for the force control. Finally, experiments were carried out to validate the designed control. The measurements of the developed MIMO-controller show good dynamics and control accuracy during transient response and at the steady state. Thus, the presented model-based control is sufficient for translational oscillatory drive applications.

REFERENCES

W. Leonhard: *Control of Electrical Drives (Power Systems)*, Springer, 2003.

Haiwei L., Jianguo Z., Zhiwei L., Youguang G: *A miniature Short Stroke Linear Actuator – Design and Analysis*, IEEE Transactions on Magnetics, 2008.

I. Choi, K. Hirata, N. Niguchi: *Design and Analysis of a Linear Oscillatory Actuator for Active Control Engine Mounts*, International Symposium on Linear Drives for Industry Applications (LDIA), 2017.

Y. Suzuki, K. Hirata, M. Kato: *Active Vibration Control of Drum Type of Washing Machine using Linear Oscillatory Actuator*, International Symposium on Linear Drives for Industry Applications (LDIA), 2017.

P. Sudwilai, K. Oka, A. Sano, Y. Hirokawa: *Vibration Control With Linear Actuator Permanent Magnet System using LQR Method*, Journal of System Design and Dynamic, 2011.

K. Sperry. *Tattoos and tattooing. Part I. History and methodology*, In: The American journal of forensic medicine and pathology 12 (4), S. 313–319, 1991.

J. Maas, T. Schulte, N. Fröhleke *Model-Based Control for Ultrasonic Motors*, IEEE/ASME Transactions on Mechatronics, Vol. 5, No. 2, S. 165-180, 2000.

Sanders, S. R.; Noworolski, J. M.; Liu, X. Z.; Verghese, G. C. *Generalized averaging method for power conversion circuits*, IEEE Trans. Power Electron. 6 (2), S. 251–259. DOI: 10.1109/63.76811.

Mönnich, O., Lehr, H., Maas, J. *Active vibration cancellation for handheld linear oscillating actuator*, 16th International Conference on New Actuators, ACTUATOR 2018.

Masoud, A., Maas, J. *Hybrid amplitude and vibration control for a small-scale linear drive with two sliders magnetically spring-loaded*, VDE IKMT, Würzburg, Germany, 2019.

Borgeest, Kai *Elektronik in der Fahrzeugtechnik: Hardware, Software, Systeme und Projektmanagement*, 3. Auflage, Wiesbaden: Springer Vieweg, 2014.

A. Gelb, W. E. Van der Velde *Multiple-Input Describing Functions and Nonlinear System Design*, McGraw Hill, New York, 1968.